Linking future precipitation changes to weather features in CESM2-LE

Kjersti Konstali [1], Thomas Spengler [1], Clemens Spensberger [1], Asgeir Sorteberg [1]

[1]Geophysical Institute, University of Bergen, and Bjerknes Centre for Climate Research, Bergen, Norway

Key Points:

- We attribute precipitation to cyclones, fronts, moisture transport axes, and cold air outbreaks in 10 ensemble members CESM2-LE in 1950-2100
- CESM2-LE adeptly represents the precipitation characteristics associated with the different weather features and their combinations
- Co-occurring weather features, associated with intense precipitation, contribute to a larger fraction of the precipitation in the future

Corresponding author: Kjersti Konstali, `kjersti.konstali@uib.no`

Abstract

Weather features, such as extratropical cyclones, atmospheric rivers (ARs), and fronts, contribute to substantial amounts of precipitation globally and are associated with different precipitation characteristics. However, future changes as well as the representation of the precipitation characteristics associated with these weather features in climate models remain uncertain. We attribute 6-hourly accumulated precipitation and cyclones, moisture transport axes (AR-like features), fronts, and cold air outbreaks, and the combinations thereof in 10 ensemble members of the CESM2-LE between 1950 and 2100 under the SSP3-7.0 scenario. We find that, despite some biases in both precipitation and weather features, CESM2-LE adeptly represents the precipitation characteristics associated with the different combinations of weather features. The combinations of weather features that contribute most to precipitation in the present climate also contribute the most to future changes, both due to changes in intensity as well as frequency. While the increase in precipitation intensity dominates the overall response for total precipitation in the storm track regions, the precipitation intensity for the individual weather features does not necessarily change significantly. Instead, approximately half of the increase in precipitation intensity in the storm track regions can be attributed to a higher occurrence of the more intensely precipitating combinations of weather features, such as the co-occurrence of extratropical cyclones, fronts, and moisture transport axes.

Plain Language Summary

Most precipitation is associated with weather features such as storms, atmospheric rivers, and fronts. Different combinations of these weather features are associated with different precipitation characteristics, but how these characteristics are represented in climate models as well as their possible future changes is not known. We attribute 6-hourly accumulated precipitation to weather features, such as storms, fronts, and atmospheric rivers, from 1950 to 2100 under a high greenhouse emission scenario in a climate model. Despite some biases, the climate model represents the precipitation characteristics associated with these weather features well. We find that the weather features with the largest contribution to precipitation in the current climate also contribute the most to future changes in precipitation. The changes are caused by changes in both frequency of occurrence and precipitation intensity.

1 Introduction

Although the global mean precipitation increase by 1-3% per degree of global warming (Held et al., 2006) is well constrained (Pendergrass & Gerber, 2016; Mitchell et al., 1987; Held et al., 2006), there are large regional differences related to local forcing, energy and water fluxes, as well as circulation features (Thackeray et al., 2018; Giorgi et al., 2019). Some of the regional differences, particularly in the extratropics, are associated with synoptic-scale features, such as cyclones, fronts, atmospheric rivers (ARs, or moisture transport axes, MTAs), and cold air outbreaks (CAOs), as these are responsible for the bulk of the precipitation (Catto et al., 2012; Catto & Pfahl, 2013; Hénin et al., 2019; M. K. Hawcroft et al., 2012; Utsumi et al., 2017; Rüdisühli et al., 2020; Konstali et al., 2024). Given that these systems are of distinct dynamical origin, they might respond differently to climate change. We therefore attribute precipitation to these weather features and quantify their contributions to the projected precipitation changes.

Attributing precipitation to these weather features establishes a link between the precipitation and the precipitation-generating mechanism, providing a more direct interpretation of the precipitation changes and the assessment of regional impacts. However, to have confidence in future climate projections, it is imperative that models simulate the current climate adequately, also with respect to weather features (Trenberth et al., 2003; M. Hawcroft et al., 2018). As the representation of precipitation characteristics associated with different combinations of cyclones, fronts, MTAs, and CAOs in climate models has not been established, we attribute precipitation to weather features in 10 ensemble members in the Community Earth System Model version 2 (CESM2, Danabasoglu et al., 2020) Large Ensemble (LE, Rodgers et al., 2021) and assess the fidelity of the model with respect to the attributed precipitation, including future changes.

Although underestimated, the precipitation associated with fronts is less underestimated than non-frontal precipitation (Catto et al., 2015). Furthermore, the frequency of fronts in CMIP5 simulations aligns well with observations (Catto et al., 2014). However, the frequency of frontal precipitation is overestimated, suggesting too many precipitating fronts (Catto et al., 2015). M. Hawcroft et al. (2018) found precipitation associated with cyclones in a high-resolution climate model to match observations quite well. However, challenges still remain regarding the representation of the weather features, as cyclones tend to be dynamically too weak in climate models compared to reanalysis (Govekar et al., 2014; Zappa et al., 2013)

In addition, precipitation remains a notoriously difficult parameter to model and its representation in climate models has been termed "dreadful" (Stephens et al., 2010). Although seasonally accumulated precipitation is quite well represented, there are still large biases in frequency and intensity, with models precipitating too often, but too little (Dai, 2006; Sun et al., 2007; Stephens et al., 2010). After a decade of model development, this issue remains in the latest generation of climate models (CMIP6, Ahn et al., 2023). However, there has not been a systematic evaluation of how biases in precipitation relate to different weather features and their combinations, with precipitation linked to weather features providing a more mechanistic understanding of precipitation biases.

Given that different weather features are characterized by different precipitation intensities (Konstali et al., 2024), changes in frequency as well as intensity of weather features can yield changes in precipitation. Cold fronts have been linked to observed precipitation trends over the Western North Atlantic (Hénin et al., 2019), while the projected decline of precipitation in the Mediterranean has been linked to a decreasing number of cyclones entering the region (Zappa et al., 2015). The precipitation increase in Western North America has been attributed to an increase in ARs (Gershunov et al., 2019) and Blázquez and Solman (2018) found that both non-frontal and frontal precipitation in the Southern Ocean has been increasing, underpinning the importance of considering multiple weather features when evaluating trends.

Utsumi et al. (2016) pointed out that even though changes in total precipitation could be small, precipitation associated with different weather features could change substantially. However, despite numerous studies, a global view of how the different weather features, and combinations thereof, contribute to regional precipitation changes is still missing. Allowing for combinations of multiple weather features yields a more detailed attribution and interpretation (Konstali et al., 2024). Considering multiple weather features co-occurring is particularly important because the combination of weather features is generally associated with more intense precipitation than when weather features occur in isolation (Catto & Pfahl, 2013; Dowdy & Catto, 2017; Prein et al., 2023; Konstali et al., 2024).

To address the outlined shortcomings, we follow the attribution method of Konstali et al. (2024) to assess how CESM2-LE, with a subset of 10 ensemble members, performs in simulating the precipitation characteristics associated with the different weather features in the present climate compared to ERA5 (Hersbach et al., 2020). We subsequently quantify precipitation biases associated with CESM2-LE attributed to the weather features. Lastly, we explore precipitation changes in CESM2-LE from a weather feature perspective to determine which combinations of weather features dominate the response and whether this response is mainly attributable to changes in the frequency or intensity of precipitation associated with the respective weather features.

2 Data and Methods

2.1 CESM2-LE

The large ensemble (LE) is initialized from the Community Earth System Model version 2 (CESM2, Danabasoglu et al., 2020) and is described in (Rodgers et al., 2021). The LE has 100 members, but only members 91-100 (the MOAR outputs) are stored with the required atmospheric fields at sufficiently high temporal resolution for our analysis. We use these 10 ensemble members for the period 1950-2100, where the period 2015-2100 follows the SSP3-7.0 emission scenario (O'Neill et al., 2016). We did all analyses for every member separately, but we present the ensemble mean unless otherwise noted.

All atmospheric fields, except for precipitation, are available at a 6-hourly temporal resolution and on a 1° grid. Precipitation is available as 3-hourly accumulated values, which we aggregate to 6-hourly precipitation centered on the 6-hourly output of the other fields.

2.2 ERA5

We use ERA5 on a 0.5°× 0.5° grid with 6-hourly resolution. 3-hourly accumulated precipitation is obtained from the short-term forecast as described in Konstali et al. (2024) and aggregated to 6-hourly data centered on the same timesteps as the historic period for CESM2-LE. ERA5 generally represents precipitation well in the extratropics, although there are some dry and wet biases in summer (Lavers et al., 2022).

2.3 Detecting weather features

To detect cyclones, we use the Wernli and Schwierz (2006) algorithm, with the modifications described in Sprenger et al. (2017). The algorithm looks for minima in sea level pressure and searches the outermost contour of a closed low-pressure system. As the algorithm occasionally also detects tropical cyclones, we refer to these features as cyclones and make no attempt to separate them further (see Konstali et al., 2024, for a discussion).

For fronts, we use the Spensberger and Sprenger (2018) algorithm, which uses the gradient of equivalent potential temperature (θ_e) and returns frontal volumes. We interpolate the temperature and humidity from model levels to 850 hPa and define the frontal objects at 850 hPa. This practice differs slightly from Spensberger and Sprenger (2018) and Konstali et al. (2024), who use three levels (925 hPa, 850 hPa, and 700 hPa) for detection, but retain the intersection of the frontal volumes at 850 hPa as their frontal objects. To test the sensitivity, we detected fronts using all three pressure levels for one ensemble member in CESM2. The frontal occurrence frequency-climatologies from the one-level and three-level frontal detections differed only by $\pm 1\%$ in the extratropics. Furthermore, the trends for the different detection methods only differed by $\pm 2\%$ along the storm-tracks, indicating that detecting fronts only at 850 hPa is sufficient. For all ensemble members, we therefore only used the equivalent potential temperature at 850 hPa to detect fronts.

The best practice of detecting fronts is to choose a threshold such that approximately 10% of the global area are considered fronts (Thomas & Schultz, 2019). However, we found the θ_e gradient-climatology between ERA5 and CESM2 to differ substantially. While the θ_e-gradient was of similar magnitude in the mid-to-high latitudes, it was weaker in the tropics in CESM2. Thus, choosing a threshold based on the 90th percentile detected considerably more fronts in the mid-to-high latitudes in CESM2 than in ERA5. Because fronts are considered a phenomenon associated with extratropical cyclones rather than tropical weather phenomena, we choose the threshold such that the climatology of frontal occurrence is similar between CESM2 and ERA5 in the midlatitudes over the stormtrack regions. We found the 95th percentile of the θ_e gradient in CESM2 suitable.

We use the MTA-detection algorithm (Spensberger et al., 2024) rather than other AR detection algorithms that are mostly based on integrated water vapour transport (IVT, Rutz et al., 2019, and references therein) and thus highly sensitive to the moisture content and global mean temperature (O'Brien et al., 2022; Shields et al., 2023). Instead, the MTA algorithm traces lines of well-defined maxima in the IVT field (Spensberger et al., 2024). We detect MTAs by first calculating the 12.5th percentile of the shear gradient of the IVT vector field in natural coordinates in the historical period and use this as our threshold, following Spensberger et al. (2024).

Given that the MTA algorithm returns lines rather than areas, we add an area with a 300 km radius around the axes in both ERA5 and CESM2 to compare frequency of occurrence across different grids. ERA5 has twice the resolution, thus the chance of an MTA occurring in a grid cell is smaller in ERA5 than in CESM2. Adding a fixed radius therefore allows for a fair comparison while keeping both datasets on their original grid.

CAOs are identified where the potential temperature difference between the sea surface (SST) and 850 hPa exceeds 3K. This definition is similar to the method by Papritz et al. (2015), albeit with a lower threshold to detect the leading edge of the CAO, following Konstali et al. (2024). We interpolate the SST and sea ice concentration field using bilinear interpolation to the regular atmospheric grid.

2.4 Attributing precipitation to weather features

We only consider accumulated precipitation >0.25 mm/6hr, which corresponds to 1 mm/day. The slightly higher threshold drastically reduces the frequency bias of precipitation (Catto et al., 2015). To attribute the precipitation to weather features, we follow the method of Konstali et al. (2024). First, we filter out precipitation associated with CAOs and attribute it to CAOs directly, because precipitation occurring within CAOs is generally weak and without clearly defined maxima (Konstali et al., 2024). We then organize the remaining precipitation into precipitation objects using a watershed algorithm (Beucher & Lantuejoul, 1979), where each object features a precipitation maximum. If one or multiple features overlap with the precipitation object, the entire object is classified as belonging to that feature or the combination of the features. With our four different weather features (cyclones, fronts, MTAs, and CAOs), we end up with 10 different precipitation categories: cyclones only (C), fronts only (F), MTAs only (A), cyclones and fronts (CF), cyclones and MTAs (CA), MTAs and fronts (AF), cyclones, MTAs, and fronts (CAF), CAOs (CAO), as well as cyclones and CAOs (CCAO). CAOs can overlap with cyclones, but not with fronts or MTAs (see Konstali et al., 2024, for a discussion).

2.5 Comparing precipitation distributions to ERA5

To compare the precipitation to ERA5, we use a modified version of the Klingaman bins (Klingaman et al., 2017)

$$b_i = \exp\left(\ln(0.005) + \left[i \cdot \frac{(\ln(120) - ln(0.005))^2}{59}\right]^{0.5}\right) + 0.245\ , \qquad (1)$$

where b is the bin and i is the bin number. We vary i between 0 and 55, and divide the interval into 300 bins to to enhance the resolution, particularly for the low intensities. The resulting bins, b, span from 0.25mm/6hr to 80mm/6hr. The bins are designed such that approximately the same number of events occur in each bin, which allows for easier comparison between observations and models with different resolutions (Klingaman et al., 2017).

2.6 Changes in precipitation

We perform a linear regression of precipitation onto global mean temperature for all ensemble members, as recommended by Pfahl et al. (2017). Regressing the changes onto temperature rather than considering different time slices removes the uncertainties associated with the different warming levels and removes some of the internal variability. In addition, regressing the changes onto the global mean temperature makes it straightforward to compare the result from CESM2 with other climate models and different forcing scenarios, particularly because CESM2 has a relatively high climate sensitivity compared to the other models (Gettelman et al., 2019).

Following Zappa et al. (2015), we decompose the changes in precipitation into contributions from frequency and intensity

$$\Delta P = \Delta N \cdot I_h + \Delta I \cdot N_h + \Delta N \cdot \Delta I \ , \tag{2}$$

where P is total precipitation, I is intensity, and N is the number of events. Δ denotes the linear trend of the respective variable per degree of warming between 1950 and 2100 and the subscript h denotes the average of the respective quantity over the historical period, which we set to be between 1950 and 1980. The decomposition in Equation (2) can also be applied in relative terms and for each of the different precipitation categories. Because the interaction term is small, we do not show it.

The intensity of total precipitation can either change due to an intensification of the precipitation categories themselves (referred to as intensity-intensity, I_I) or due to relatively more precipitation falling within a category associated with relatively stronger precipitation (referred to as intensity-frequency, I_F). We disentangle these contributions into

$$\Delta I_I = \sum_{k=0}^{k=9} (\Delta I_k \cdot F_h / I_{tot_h}) \tag{3}$$

$$\Delta I_F = \sum_{k=0}^{k=9} (\Delta F_k \cdot I_h / I_{tot_h}) \ , \tag{4}$$

where we sum over all the weather categories (denoted by subscript k). I_{tot_h} is the total intensity irrespective of the precipitation categories and F is the frequency of precipitation events.

3 Representation of current climate

3.1 Precipitation

The climatology of total precipitation is similar in CESM2 compared to ERA5 (Figure 1a,b, Figure 2a,b, and Figure S1), where current climate refers to the period between 1979 to 2014. However, in the North Atlantic, CESM2 overestimates precipitation compared to ERA5 south of Iceland (30-50%) and the fine precipitation structure in ERA5 over the Gulf Stream is not evident in CESM2. Along the North Pacific stormtrack, the total precipitation is slightly overestimated in DJF (10-15%) while it is underestimated downstream of the southern flank of the stormtrack in JJA in the Northwest Pacific (30-50%). In the Southern Hemisphere, CESM2 precipitates too much between 30°S to 60°S; and while the bias is present in both seasons, it is most pronounced in JJA. In contrast, precipitation is underestimated over much of the NH continents in summer, particularly over the Great Plains in the US and over Europe. However, the overall largest biases are in the tropics, particularly south of India and over Brazil.

Precipitation frequency is overestimated in the zonal mean at all latitudes in the winter hemisphere and is slightly more variable in the summer hemisphere (Figure 1e,f and Figure 2e,f in addition to their respective panels). Note that because we use a relatively high precipitation threshold (0.25 mm/6hr), we have most likely reduced the precipitation bias considerably (Catto et al., 2015). In the extratropics, the largest frequency bias in the North Atlantic is found just south of Iceland, coincident with the overestimation of the total precipitation. Here, precipitation occurs more than 80% of the time in CESM2, but only 60% in ERA5 in DJF (Figure 1e,f). There is no similar bias in JJA. Precipitation is also overestimated in the North Pacific and in the Southern Ocean, but not as severely as in the North Atlantic for DJF. Over the subtropical oceans, the frequency is underestimated in CESM2 by more than 50% compared to ERA5, while there are large positive and negative frequency biases close to the ITCZ, probably related to double ITCZ biases.

In contrast to frequency, intensity is underestimated in the mean at all latitudes, but most in the zonal mean at 35°N to 40°N in the NH in JJA (Figure 2c,d) and at 30° in DJF (Figure 1c,d). In the SH, the precipitation intensity is underestimated over the entire South America, except along parts of the Andes in DJF. Although the intensity is underestimated over large parts of both the North Atlantic and the North Pacific Ocean, the intensity bias is most pronounced over the continents in the summer hemisphere. For example, precipitation intensity over the Great Plains in JJA is underestimated by more than 1mm/6hr (corresponding almost 50%, Figure 2c,d). Precipitation in this region is mainly associated with mesoscale convective systems (Feng et al., 2019), which are known to be poorly represented in climate models (Kooperman et al., 2014). The intensity is also underestimated over the Alps, as well as most of Africa and Australia, both in DJF and JJA, likely related to parameterized convection (Stevens & Bony, 2013) as well as poorly resolved topography (i.e., Munday & Washington, 2018).

3.2 Weather feature climatology

Both the qualitative patterns of cyclones, fronts, and MTAs are well represented by CESM2 in the extratropics for both seasons (see supplement for details). There are too many cyclones, particularly in the high latitudes, and there are too many fronts. MTAs are well represented in the stormtrack regions, where they represent moisture convergence along cold fronts, similar to atmospheric rivers (Dacre et al., 2015; Spensberger et al., 2024). Low-level jets (LLJ), such as the Great Plains LLJ from the Gulf of Mexico towards the Great Plains and the South American LLJ on the eastern side of the Andes are less clearly defined in CESM2 than in ERA5.

There are larger biases associated with CAOs than the other features. In DJF, there are large biases in both the North Pacific and the North Atlantic (Figure S2). The overall frequency of CAOs is overestimated in CESM2, particularly south of Iceland and in the Northwest Pacific. In contrast, the CAO frequency is underestimated both over the Kuroshio extension as well as over the Gulf Stream (Figure S2). In JJA, there are no CAOs in the NH, but the frequency is overestimated in the SH (Figure S3). That CAOs are less well represented is most likely due to SST biases in CESM2 (Danabasoglu et al., 2020). Furthermore, the maximum frequency bias of CAOs coincides with the location of maximum precipitation frequency bias in the North Atlantic, indicating that this bias can most likely be linked to CAOs occurring too frequently.

3.3 Precipitation attribution to weather features

The spatial distribution of precipitation attributed to weather features compares well with ERA5 (Figure S2 and Konstali et al. (2024), their Figure 4). Considering the entire precipitation distribution rather than aggregated results, we analyze how much the different intensity bins of the precipitation distribution (Klingaman et al., 2017, Equation 1) contribute to the total precipitation in the different precipitation categories. Note that the shape of the distribution is quite sensitive to the number of bins, but that the

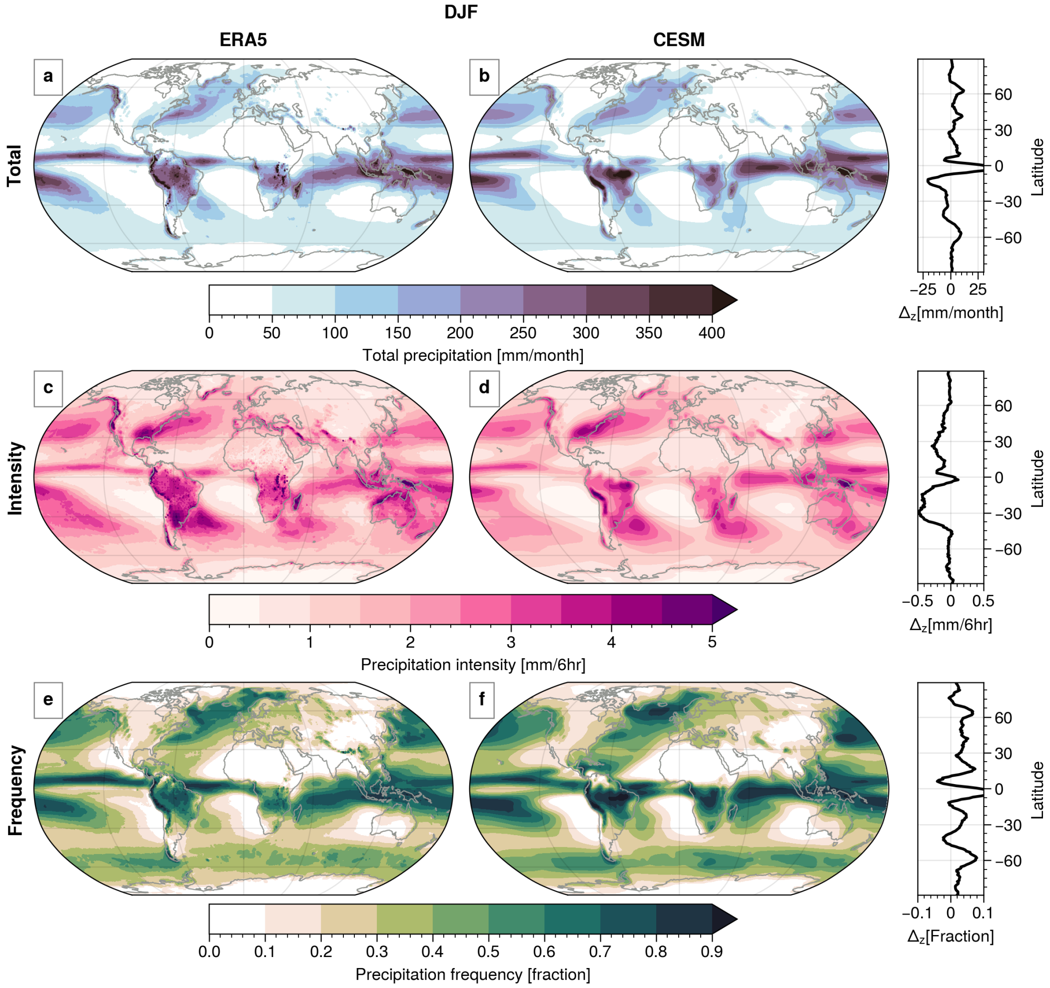

Figure 1. Comparison of ERA5 to the CESM2 in DJF (1979-2014) in terms of total precipitation (a,b), average precipitation intensity of precipitation events exceeding 0.25 mm/6hr (c,d), and frequency of precipitation events exceeding 0.25 mm/6hr (e,f). The panels on the right show the zonal mean difference (denoted Δ_z) between CESM2 and ERA5 for total precipitation, intensity and frequency.

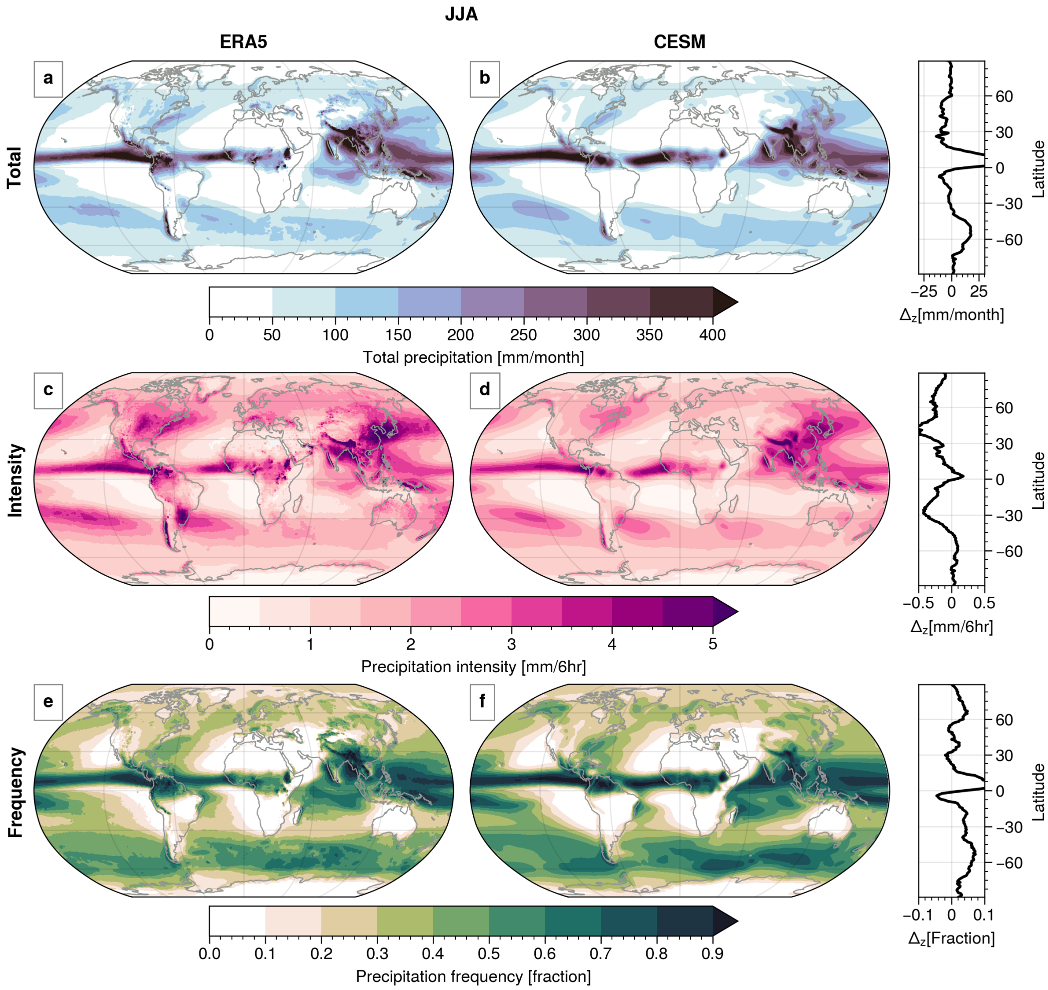

Figure 2. As Figure 2, but for JJA.

difference between CESM2 and ERA5 remains the same. We aggregate into latitude bands to assess whether the precipitation characteristics associated with the different weather features are comparable between CESM2 and ERA5 and to determine whether CESM2 precipitates for the right reasons.

3.3.1 Midlatitudes (30°-60°)N/S

In CESM2, unclassified (U) is the most bottom-heavy precipitation distribution in the midlatitudes, that is, the largest contribution to this category comes from intensities below 1mm/6hr (Figure 3a). The mean precipitation in the unclassified category is 0.9mm/6hr, which is slightly more intense within the categories for cyclones only (C, 1.1 mm/6hr), fronts only (F, 1.5mm/6hr), and MTAs only (A, 1.5 mm/6hr). The co-occurrence of multiple weather features is associated with more intense precipitation, and the most intense precipitation occurs when all three weather features overlap (CAF, 3.3mm/6hr). CAF contributes most to precipitation in the midlatitudes (31%) followed by the co-occurrence of MTAs and fronts (AF, 20%). Note that the thin, dashed lines on the right sides of the contribution graph are the individual ensemble members and that the spread is generally very small.

Despite some biases in terms of both precipitation (Figure 1, Figure 2) and frequency of features (Figure S2, S3), the different precipitation categories contribute similarly to total precipitation in CESM2 and ERA5 (Figure 3a). The largest discrepancy is within CAF, which contributes 31% in the total precipitation in CESM2, while only 28% in ERA5. The mean precipitation intensity is underestimated in all the different categories, except for CAOs, where precipitation intensity is overestimated. In contrast to Catto et al. (2015), we do not find that precipitation associated with fronts is underestimated less than the other precipitation categories. Rather, we find the intensity bias to be a systematic feature across all the precipitation categories.

3.3.2 Northern Hemisphere high latitudes (>60°N)

Precipitation intensity is generally smaller in the high latitudes compared to the midlatitudes (Figure 3b). Most precipitation comes from cyclones only (C, 21%), followed by unclassified (U, 15%). As in the midlatitudes, unclassified is the most bottom-heavy precipitation category with an average precipitation rate of 0.6 mm/6hr. Relatively less precipitation comes from CAF in the high latitudes compared to the midlatitudes, but CAF is still associated with the most intense precipitation (2.1 mm/6hr).

While most precipitation comes from cyclones only (C) in both ERA5 and CESM2, the contributions to total precipitation differ more in the Arctic than in the midlatitudes (Figure 3b). Less precipitation comes from unclassified in CESM2 compared to ERA5 (15% compared to 21%), whereas relatively more is associated with cyclones and fronts (CF, 20% compared to 15%) and cyclones, MTAs, and fronts (CAF, 19% compared to 15%). This discrepancy is consistent with the more frequent occurrence of fronts and MTAs in high latitudes (Figure S2, S3). However, many of the additional fronts and MTAs are associated with cyclones and precipitation, indicating that the detection of these weather features is dynamically sound. Despite the comparable mean precipitation rate for total precipitation (1.2 mm/6hr in ERA5 vs 1.1 mm/6hrs in CESM2, rightmost contribution-graph in Figure 3b), there are too many drizzle events ($<$ 0.5 mm/6hr), mainly associated with events occurring without any weather feature in CESM2 (Figure 3b, U).

3.3.3 Tropics (30°S-30°N)

The precipitation distributions in the tropics look vastly different from those in the mid- and high latitudes in CESM2 (Figure 3c). Most precipitation is associated with MTA only (A, 36%), followed by unclassified (U, 33%). Despite the relatively higher precipitation intensities in the tropics in U compared to the mid- and high latitudes, U is still the most bottom-heavy category in CESM2.

In general, there are larger biases in the tropics than in the other regions. More precipitation is associated with fronts in ERA5 than in CESM2, related to the lower frequency of fronts in the tropics (Figure S2, S3), though the precipitation attribution is designed to work best in extratropics (Konstali et al., 2024).

4 Projected precipitation changes

As CESM2 has proved to simulate precipitation, weather features, and the precipitation associated with the weather features reasonably well, CESM2 appears to be a suitable tool to investigate precipitation changes from a weather perspective. Analyzing precipitation from a weather perspective has the advantage that we are able to link the precipitation changes directly to the weather features causing the change, thus obtaining a more mechanistic understanding of the precipitation changes.

4.1 DJF

Globally, precipitation increases by 1.5%/K in CESM2, which is on the lower end of the range of the expected precipitation change (Held et al., 2006). However, the spatial pattern of the change is highly variable (Figure 7a). The midlatitude dry regions feature a drying, consistent with the results from the CMIP6 models (Douville et al., 2023), while the midlatitude stormtrack, as well as the continents, show a general wettening. This pattern is consistent with the dry-get-drier-wet-get-wetter paradigm that explains the projected pattern of precipitation over the ocean (Allan et al., 2010; Chou et al., 2013). The exception is the "North Atlantic Warming Hole" (i.e., Drijfhout et al., 2012; Gervais et al., 2019) between Greenland and Iceland, within which precipitation is projected to decrease.

The precipitation change can be decomposed into the contributions from intensity and frequency using Equation (2). The regions where the total precipitation trend is negative coincides with the negative frequency trend, consistent with Polade et al. (2014) (Figure 4c). In general, the frequency trend is negative over much of the SH and over the NH oceans, whereas it is positive in the tropics, over the NH continents, and in the high latitudes.

In contrast to frequency, the intensity contribution is positive everywhere in DJF over land, while it is negative over most of the subtropical oceans (Figure 4b). Within the NH stormtrack, the changes in intensity contribute more to the total change in precipitation compared to the changes in frequency (from 3 to 5%/K compared to from -3 to 1%/K). The exception is the North Atlantic Warming Hole, where both changes in intensity and frequency contribute approximately equally to the negative change. While the intensity contribution is positive almost everywhere in the high latitudes, it is negative over the Atlantic sector in the Arctic, where it decreases between -5%/K to -3%/K.

4.2 JJA

The global mean change in precipitation varies little between JJA and DJF, but the spatial pattern differs (Figure 4d). In JJA, the drying trends extend over most of Europe up to 60°N and far into Russia. However, exactly how far north the drying will extend in Europe is uncertain (Ritzhaupt & Maraun, 2023). North America, Canada, and the Great Plains become drier, whereas the precipitation increases in Western North America and in some regions around the Gulf of Mexico.

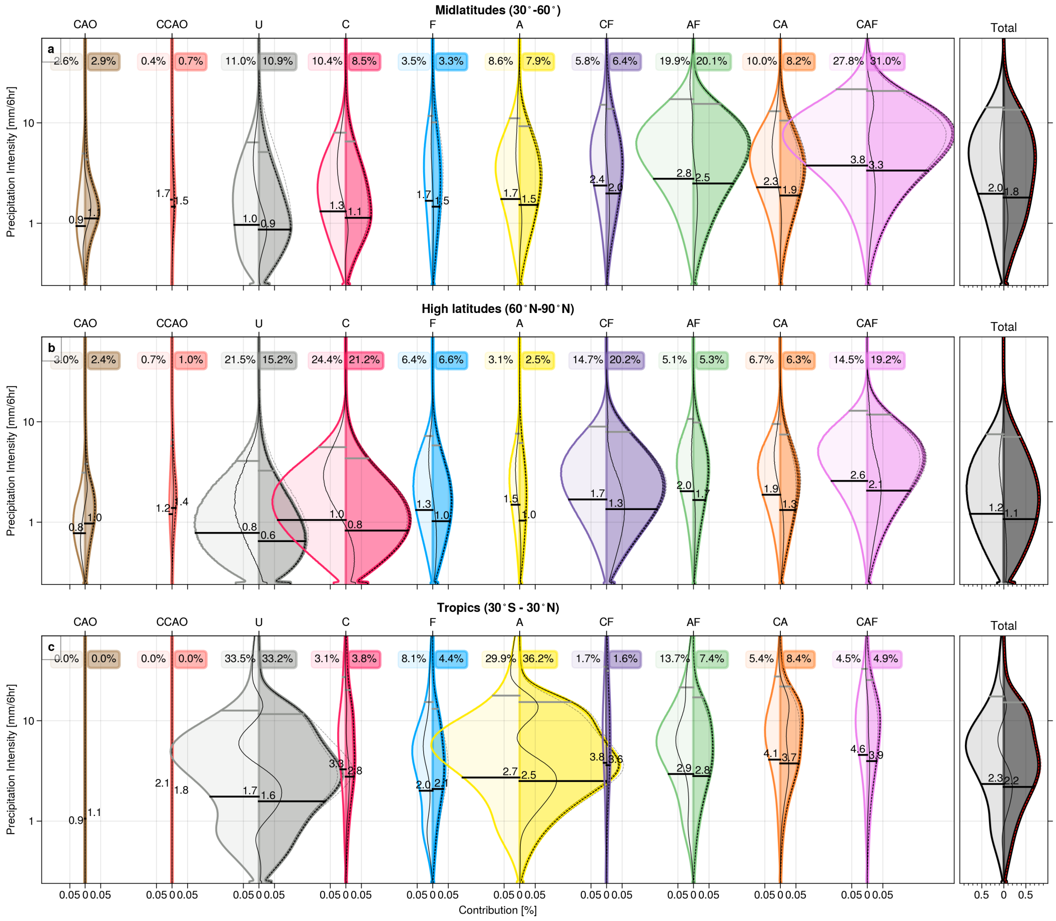

Figure 3. Contribution of respective intensity bins in the different categories to the total precipitation (irrespective of categories) in a) the midlatitudes, b) the NH high latitudes, and c) the tropics. The left distribution is ERA5, and the right is the CESM2-LE. Note that the total distribution is on a different x-axis and that the y-axis is logarithmic. Black horizontal lines within distributions mark the mean precipitation within the category, and the number above gives the mean intensity, while the gray line gives the 99.9th percentile. The thin black curve within the distribution is the difference between the CESM2-LE and ERA5 distributions, while the dashed curves on the right side of the distribution mark the different ensemble members. The number on the top gives the contribution from the different categories to the total precipitation for ERA5 (left) and CESM (right). CAO is precipitation in Cold Air Outbreaks, CCAO precipitation occurring within CAOs and cyclones, U is unclassified, C is cyclones only, F is fronts only, A is MTAs only, CF is cyclones and fronts, AF is MTAs and fronts, CA is cyclones and MTAs and CAF is cyclones, MTAs and fronts.

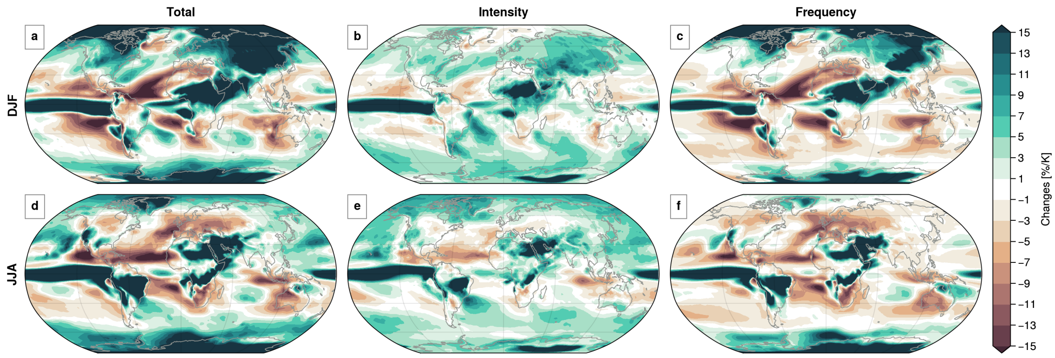

Figure 4. Changes in total precipitation in DJF and JJA (a,d) and the contribution frequency (b,e) and intensity (c,f).

Similar to DJF, the decrease in frequency contributes most to the negative change in the NH midlatitudes (Figure 4f). The exception is Western North America and the Gulf of Mexico, where the total precipitation is increasing, concomitant with an increase in frequency.

The changes in intensity, on the other hand, are positive almost everywhere, except for the southernmost part of the North Atlantic and in the subtropical SH (Figure 4e). Over most of the North Atlantic, there is a decrease in both frequency and intensity. This is in contrast to the North Pacific stormtrack, where most of the increase in precipitation is due to an increase in the intensity of precipitation. In general, the intensity contribution is smaller than that of frequency, consistent with Polade et al. (2014).

5 Changes in the frequency of occurrence of weather features

As different weather features are associated with different precipitation intensities (Figure 3), changes in the frequency of occurrence of the weather features can have an impact on the total precipitation change. We thus first discuss trends in the occurrence of weather features and then relate them to precipitation trends in section 6.

Along the North Atlantic stormtrack in DJF, the cyclone occurrences increase over the British Isles (> 1%/K) while the number decreases over the Mediterranean (-1.5%/K to -1%/K, Figure 5a). Our results are largely consistent with Zappa et al. (2013), except that we do not find a decrease in cyclones close to Greenland. Akperov et al. (2019) found a large model spread in cyclone trends in the region. In the North Pacific stormtrack and in the SH, cyclone occurrence shifts poleward, while the North Atlantic shows an extension of the stormtrack into Europe, consistent with Priestley and Catto (2022) (Figure 5a). In JJA, the number of cyclones decreases in the North Atlantic (-1.5%/K to -0.5%/K), but increases in the North Pacific (0.5%/K, Figure 5b).

In the NH in DJF, the frequency of fronts increases everywhere (Figure 5c), with the largest increase occurring just off the coast of the British Isles, consistent with the maximum increase in cyclone frequency (Figure 5a). The frequency of fronts increases less in the North Pacific than in the North Atlantic, whereas the frontal frequency increases everywhere in DJF in the SH midlatitudes.

In JJA, in contrast, the frequency of fronts decreases off the coast of West Antarctica, while it slightly increases everywhere else in the SH (Figure 5d). In the NH, fronts become more frequent everywhere except for a decrease over central North America. The largest increase in front frequency occurs along the coastlines in the summer hemisphere.

This is most likely related to the thermal inertia of the ocean, with the land warming faster, increasing the existing land-sea contrast.

That fronts are predominately increasing is in contrast to Catto et al. (2015), who found the frequency of fronts to decrease. However, the overall number of our detected front objects in the midlatitudes does not change (not shown). Thus, the increase in the frequency of fronts is related to fronts becoming larger or more elongated. As Catto et al. (2015) considered fronts as lines and not areas, their method would be less sensitive to an increase in size, unless fronts become substantially longer rather than wider. Furthermore, as Catto et al. (2015) considered annual mean changes, our results are not directly comparable.

The occurrence of MTAs decreases south of Iceland with increasing global mean temperatures, while it increases over Europe and into Russia in DJF (Figure 5e). There seems to be a poleward shift of the MTA frequency in the North Pacific and the SH stormtracks, consistent with the poleward shift of cyclones (Figure 5a,e).

In JJA, MTAs show a substantial increase in frequency in the Arctic (2%/K), most likely due to the increasing moisture content (Figure 5f). However, there is a narrow band of decreasing frequency extending diagonally from Florida to the British Isles. Such a pattern is not visible in the North Pacific, where MTAs increase everywhere poleward of 30°N. The difference in response in MTAs could potentially be related to the difference in cyclone frequency changes between the North Atlantic and North Pacific in JJA (Figure 5b).

Although there are quite large changes in the MTAs, the pattern is mainly an amplification of the existing pattern (Figure S2, S3). The relative changes are small, particularly over the stormtrack regions where MTAs are frequent (not shown). The changes in MTAs are consistent with the calculated changes in frequency of atmospheric rivers using the TECA-BARD algorithm (O'Brien et al., 2020), whereas AR detection algorithms using an integrated water vapour threshold show a more uniform increase everywhere (O'Brien et al., 2022).

Of all the weather features we consider, CAOs change the most (Figure 5g,h). The frequency decreases by more than 2%/K in DJF over much of the North Atlantic and North Pacific and the frequency moves poleward as the sea ice edge retreats (Figure 5g). Thus, CAOs become more frequent in areas that are currently ice-covered. A similar pattern is also visible in the SH in JJA, where CAOs move poleward as the sea ice edge retreats (Figure 5h).

6 Linking precipitation changes to weather features

6.1 Changes in precipitation intensity due to changes in occurrence or intensity of weather features

The intensity of total precipitation (irrespective of the precipitation categories) can occur in two ways: Either precipitation in the different categories becomes more intense, or there is a shift in which categories contribute to the total precipitation. We refer to the former as the intensity-intensity, and the latter as intensity-frequency, and calculate their contributions as in Equation 3 and Equation 4. As the different categories are associated with different mean intensities (Figure 3), a shift in the contribution of the categories can cause a change in precipitation intensity, despite no changes in precipitation intensity within the categories.

In DJF, there is an intensification of precipitation within the respective precipitation categories (intensity-intensity) over much of the NH continents (Figure 6a). In contrast, over the subtropics, intensity-intensity mostly decreases. A decrease in the sub-

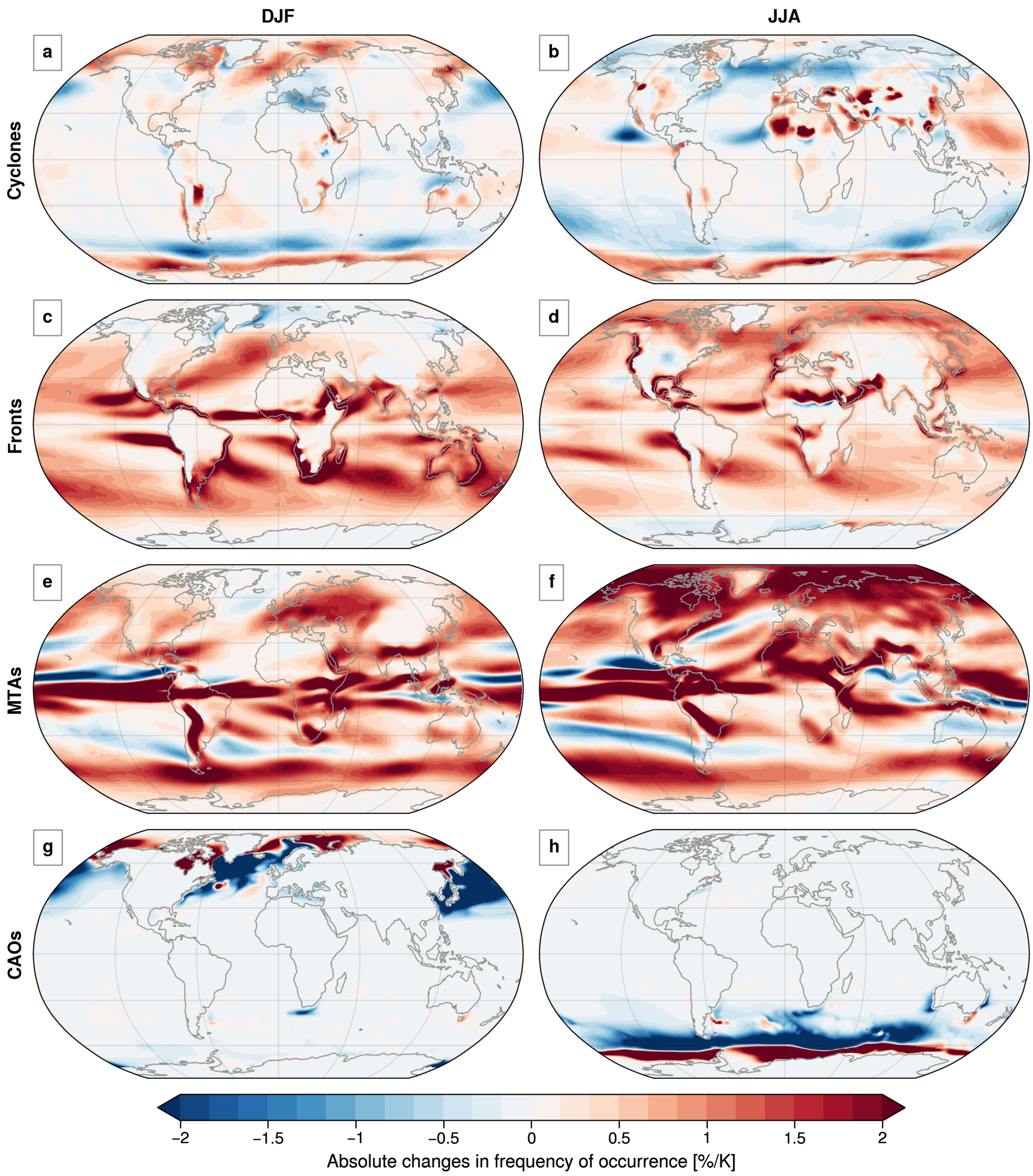

Figure 5. Absolute changes in frequency of occurrence of features given in %/K. a,b) Cyclones for DJF and JJA, c,d) changes in fronts in DJF and JJA, e,f) in MTAs in DJF and JJA, and g,h) changes in CAOs in DJF and JJA.

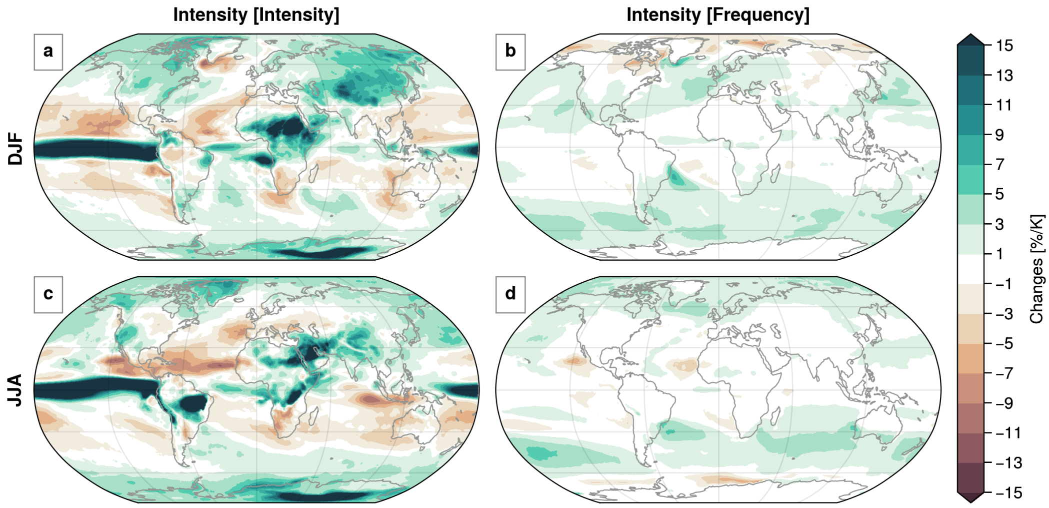

Figure 6. The contribution to total intensity change from changes in intensity-intensity in DJF (a) and JJA (c) and from intensity-frequency in DJF (b) and JJA (d).

tropical intensity-intensity is consistent with Scheff and Frierson (2012), who found that the precipitation intensity decrease was due to the dynamic contribution associated with the expansion of the Hadley cell.

In comparison to intensity-intensity, the intensity-frequency contribution to intensity changes has a smaller spatial variability in DJF (Figure 6), with a positive contribution to the intensity increase (between 1%/K and 3%/K) over much of the stormtrack regions. Northward of 60°N, the intensity-frequency contributes negatively to the change, and the decrease is particularly strong at the northernmost edge of the Barents Sea, east of Greenland, and over the Bering Strait, where it decreases between -5%/K and -3%/K. A decrease in the intensity-frequency indicates that the weakly precipitating categories are projected to contribute more to the precipitation in the future. In the high latitudes, this implies an increase in the unclassified (U) or cyclones only (C) categories and a decrease in the contribution from the combined categories, for example CAF (Figure 3).

The most notable difference between JJA and DJF is that the intensity-intensity decrease in JJA is more widespread over the continents (Figure 6). Intensity-intensity decreases over the North Atlantic and the Mediterranean, whereas it increases poleward of 30° in the North Pacific, probably also related to the expansion of the Hadley cell (Scheff & Frierson, 2012), while the decrease over Eastern North America may be related to the decreasing frequency of fronts and cyclones (Figure 5b,c).

The intensity-frequency is generally positive, also in JJA (Figure 6). Unlike in JJA, the contribution from intensity-frequency is positive in the Arctic, indicating that in winter, more precipitation is associated with the combined categories rather than cyclones only (C) or unclassified (U) (Figure 3). Similar to the Arctic in DJF, intensity-frequency contributes negatively along the coast of Antarctica.

6.2 Midlatitudes

6.2.1 Ocean

In DJF, most of the positive precipitation change over the North Atlantic is caused by the co-occurrence of cyclones, MTAs and fronts (CAF, Figure 7j). MTAs and fronts

(AF) contribute the second-most, but the maximum contribution is displaced equatorward off the maximum contribution of CAF. Thus, the precipitation categories that contribute the most to precipitation in the current climate also contribute the most to the change in precipitation (Figure S4), consistent with Utsumi et al. (2016). On the other hand, MTAs only (A) and cyclones and MTAs (CA) contribute negatively to the precipitation changes, in line with the more frequent occurrence of fronts (Figure 7). Over the North Atlantic Warming Hole, where total precipitation is decreasing, the bulk of the decrease occurs in the CAO category (Figure 7). A decrease in CAO precipitation is consistent with Gervais et al. (2020), who found that the decrease in precipitation in the North Atlantic Warming Hole is associated with a decrease in fluxes and lower SST.

The pattern is relatively similar in the North Pacific stormtrack in DJF, with CAF and AF contributing to the bulk of the precipitation increase (Figure 7i). However, there is a clear poleward shift in the contributions from CAF and AF consistent with the poleward shift of the stormtrack. The categories for cyclones only (C), cyclones and MTAs (CA), and MTAs only (A) show a decrease in the North Pacific, while CAO decreases over the Kuroshio extension.

Along both NH stormtracks, there is a projected decrease in the frequency of precipitation and an increase in intensity, of which a substantial fraction is due to the intensity-frequency contribution in DJF (Figure 6a,b). The intensity-frequency contribution is consistent with the increased contribution from CAF, as well as a decrease from CA, A, and C, as CAF is associated with relatively more intense precipitation (Figure 3). In addition, the CAF and AF intensities increase by 3-5%/K over much of the NH stormtracks (Figure S6).

The change in the SH stormtrack is very similar to the North Pacific, but there is little seasonality. The bulk of the change is due to changes in CAF and AF. Similar to the North Pacific, most of the CAF and AF increase occurs poleward of the historical maxima, consistent with the poleward shift of the SH stormtrack. C and A contribute negatively to the change. There is a larger increase in CAF and AF in JJA than in DJF (Figure 7, Figure 8), but the intensity change is similar between the seasons, indicating that the difference between seasons mainly stems from changing frequency (Figure S8j, S10j).

Unlike in the SH stormtrack, there are large seasonal differences in the NH stormtrack, particularly in the North Atlantic (Figure 8). The total precipitation decrease is much more widespread in JJA than in DJF in the North Atlantic. Most of the decrease comes from a decrease in frequency (-4%/K), although there is also a decrease in intensity over the North Atlantic (-0.4%/K, Figure 4e,f). The largest contribution to precipitation in the present climate comes from CAF and AF (Figure S4), but CAF contributes negatively to the projected precipitation change, consistent with the decrease of cyclones (-1.5%/K, Figure 5b). The decrease in CAF is partly compensated by an increase in AF. Nonetheless, the precipitation in the categories related to cyclones decreases in the North Atlantic, yielding a net precipitation decrease (-3.6%/K). The difference in the frequency change of cyclones between DJF and JJA in the North Atlantic seems to explain almost the entire difference in the seasonality of the precipitation changes.

In contrast to the North Atlantic, both CAF and AF increase in the North Pacific in JJA (Figure 8), but there is no poleward shift of the contribution, unlike in DJF. Changes in CAF along the North Pacific stormtrack are associated with both frequency and intensity (6.5%/K and 4.6%/K, respectively, Figure S8, S9). The category for cyclone and front (CF) contributes substantially to the total precipitation change (15%), but mainly south of the maximum contribution from CAF. In fact, some of the precipitation associated with CAF and AF occurs south of 30°N. This precipitation is likely associated with tropical cyclones (TC), which we do not explicitly detect in our analysis (see Kon-

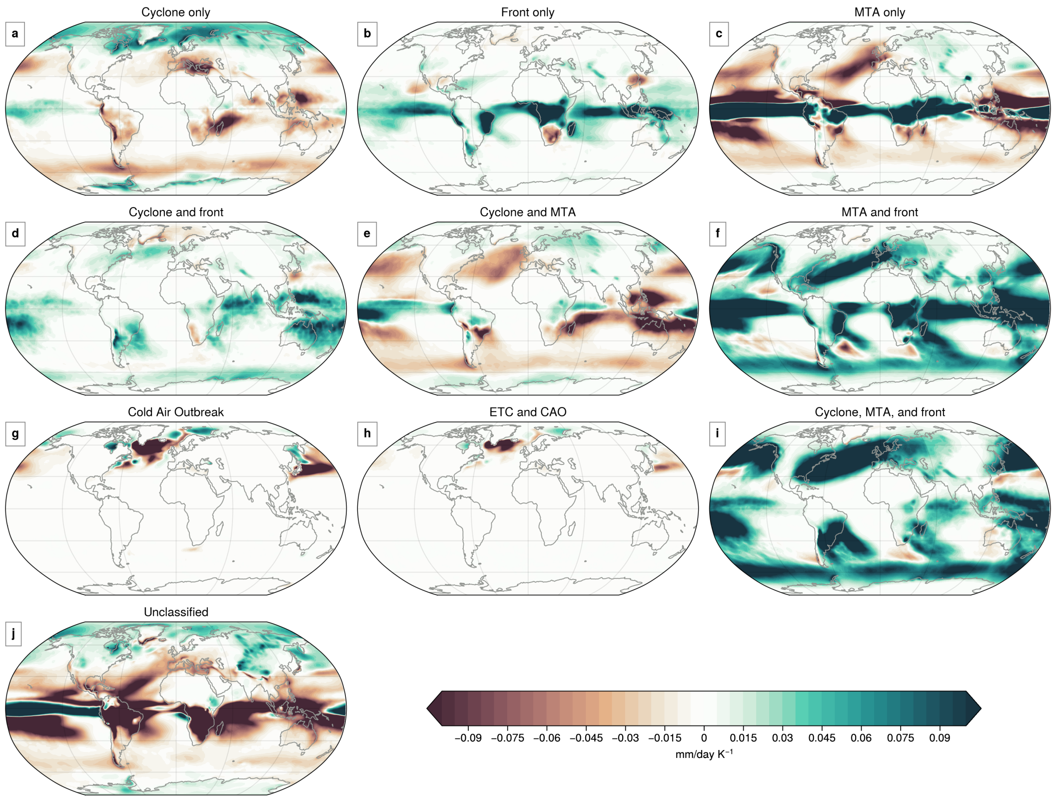

Figure 7. The absolute change in precipitation from the different categories in DJF.

stali et al., 2024, for a discussion). An increase in TC precipitation in this region is consistent with Utsumi et al. (2017).

6.2.2 Mediterranean and continents

Downstream of the stormtrack and over the continents in DJF, precipitation associated with cyclones, MTAs, and fronts (CAF, AF) increases (Figure 7). CAF and AF contribute most to the precipitation change in Europe (72% and 40%, respectively), mainly due to an increase in frequency (15%/K, Figure S7). The precipitation increase in Western North America is mainly due to AF (figure 7f), which increases in Western North America both in terms of frequency and intensity (6%/K and 3%/K, respectively, Figure S6, S7).

In contrast, in JJA, precipitation decreases over most of the NH continents, except for east Asia, Western North America, and around the Gulf of Mexico (Figure 4d). The decrease is mainly due to the decrease in the frequency of precipitation, which decreases everywhere where the total precipitation decreases (Figure 4f). Most of the decrease over North America and Russia is linked to a decrease in cyclones only (C), cyclones and fronts (CF), cyclones, MTAs, and fronts (CAF), and unclassified (U), while the decrease over Europe is mostly due to C (Figure 8a). In Western North America, where precipitation is increasing, both the frequency and intensity of CAF and AF contribute positively to the precipitation change in JJA (Figure 8).

The negative precipitation trend over the Mediterranean in DJF is mainly due to a decreasing trend in cyclones (Figure 5a), consistent with Zappa et al. (2015). The fre-

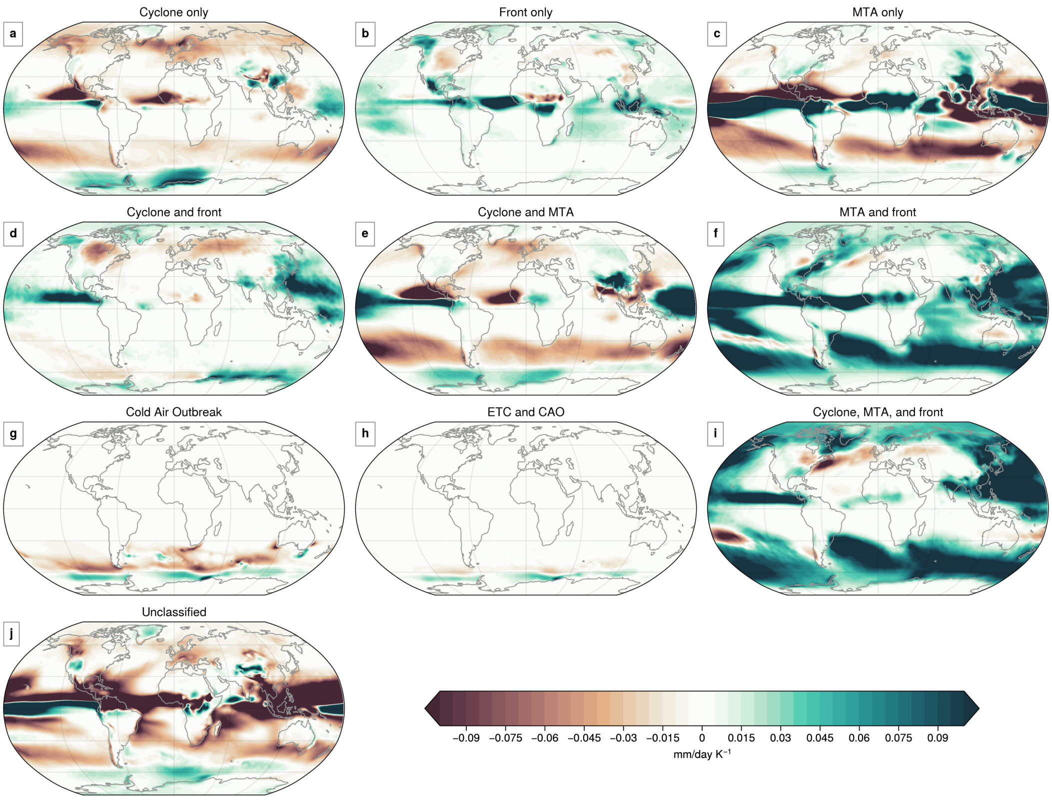

Figure 8. As Figure 7, but for JJA.

quency of cyclones entering the Mediterranean decreases with 0.5%/K (Figure 5a), leading to cyclones only (C) precipitation occurring almost 20%/K less often (Figure S10).

Whereas cyclones contribute most to the decreasing trend in DJF, unclassified (U) decreases the most in JJA in the Mediterranean (Figure 8). Given that the precipitation in U around the Mediterranean is mostly convective, the decrease in U can mainly be explained by a widening of the subtropical high and associated mean subsidence (Laua & Kim, 2015), yielding an increase in static stability and convective inhibition (CIN) in a future climate (Dai et al., 2020). As unclassified is not associated with strong external forcing, locally forced convective events may not be able to overcome the increased CIN and increased stability, yielding a decrease in the frequency of unclassified precipitation events.

6.3 High Latitudes

Precipitation increases by almost 17%/K poleward of 60°N in DJF, making it one of the fastest-increasing regions worldwide (Figure 4a,d). Cyclones only (C) and unclassified (U) precipitation contribute to almost 70% of the total change in the high latitudes and are thus both dominating precipitation in the current climate and the projected change. Most of the change in U and C is associated with an intensity change (Figure S6). The occurrence of relatively more precipitation within these two weakly-precipitating categories (Figure 3) is consistent with the decrease in intensity-frequency poleward of 60°N in DJF (Figure 6) and likewise consistent with the general increase in the number of cyclones poleward of 60°N in DJF (Figure 5a).

In JJA, most of the precipitation increase stems from the CAF and AF categories, while relatively less occurs within C and U (Figure 8a,j,i). Most of this increase is due an increase in their frequency (Figure S10), consistent with a more frequent occurrence of both fronts and MTAs intruding into the interior Arctic (Figure 5d,f).

7 Summary and concluding remarks

We analyzed precipitation in 10 ensemble members of CESM2-LE and attributed it to cyclones, fronts, moisture transport axes (MTA), and cold air outbreaks (CAOs), as well as their combinations. Qualitatively, CESM2 captures the precipitation patterns well, but the model precipitates too often and too little. CESM2 places the weather features mostly in the correct locations with frequencies similar to ERA5, but particularly CAOs are associated with substantial biases. Some of the precipitation bias can be directly linked to biases in the representation of weather features. For instance, the too frequent occurrence of CAOs south of Iceland is associated with a large precipitation frequency bias.

Despite these issues, CESM2 performs well in capturing the precipitation characteristics of the different precipitation categories as well as the differences between regions. The different precipitation categories contribute approximately the same towards the total precipitation compared to ERA5, but the mean intensity is underestimated across all the categories. This points to a systematic bias; but unlike Catto et al. (2015), who found frontal precipitation intensity to be less underestimated, we find all categories to be approximately equally underestimated. Our results might still be consistent with Catto et al. (2015) when considering the varying average intensities per category. In CESM2, more frontal precipitation is part of the CAF category, which on average precipitates much more than the other frontal categories, thus decreasing the bias in frontal precipitation intensity.

The contribution from the frequency decrease dominates the regions where the overall precipitation trend is negative, consistent with Polade et al. (2014). In contrast, the intensity change is mainly positive. However, because different weather features are associated with different mean intensities, a shift in the dominant category could lead to an apparent intensity increase, despite there being no intensification of the individual categories. We find this contribution, which we term intensity-frequency, to contribute more than 50% of the total intensity change along the stormtracks, with the contribution predominately being positive. This indicates a shift towards a larger contribution from the relatively more intensely precipitating categories, in addition to the categories themselves intensifying.

In the stormtrack region, precipitation associated with cyclones, MTAs, and fronts (CAF) contributes most to the projected precipitation change. As CAF is the most intensely precipitating category, an increase in the contribution from CAF is consistent with the positive intensity-frequency trend. MTAs and fronts (AF) contribute the second most to the precipitation change. The changes in CAF and AF are mainly due to changes in their frequency. On the other hand, cyclones only (C), MTAs only (A), cyclones and MTAs (CA), and unclassified (U) all contribute negatively to precipitation changes over the stormtracks, both in JJA and DJF. Thus, despite there being fewer cyclones, more of these cyclones co-occur with MTAs and fronts.

Over the continents, frequency trends are negative in the summer season and positive in the winter season (at least poleward of 40° NH in DJF). The intensity increase is mainly positive over the continents in DJF. Downstream of the stormtracks, CAF and AF contribute the most to precipitation. Overall, our findings are consistent with Utsumi et al. (2016), who found that features that contribute the most to precipitation in the current climate also contribute most to the projected precipitation changes.

As we have only used one climate model, the question of whether all CMIP6 models simulate the precipitation characteristics with the different weather features equally well remains. Furthermore, the results may be sensitive to the feature detection algorithms used, as pointed out by Shields et al. (2023) for the different atmospheric river detection algorithms.

Our results show that the different precipitation categories respond differently to the projected climate changes. This suggests that, in addition to the availability of moisture, other factors determine how efficiently the different weather systems produce precipitation. While this study focused on changes in mean precipitation, future work should entail changes across the entire distribution, as extreme precipitation is expected to increase more than the mean.

8 Open Research

The CESM2-LE ensemble members are available in the Climate Data Gateway at NCAR `https://www.earthsystemgrid.org/dataset/ucar.cgd.cesm2le.atm.proc.6hourly_ave.html` and `https://www.earthsystemgrid.org/dataset/ucar.cgd.cesm2le.atm.proc.3hourly_ave.html`. All feature detection algorithms as well as the attribution method can be found in Dynlib (`https://zenodo.org/records/10471187`; Spensberger, 2024).

Acknowledgments

KK was supported by UiB. CS was supported by Research Council of Norway project "Atmosphere-Sea Ice interactions in the new Arctic" (project number 302934). TS was supported by Research Council of Norway project "Bias Attribution Linking Moist Dynamics of Cyclones and Storm Tracks" (project number 324081). AS was supported by the NFR KeyClim project (project number 295046) and UiB. We would like to acknowledge high-performance computing support from Cheyenne (doi:10.5065/D6RX99HX) provided by NCAR's Computational and Information Systems Laboratory, sponsored by the National Science Foundation.

References

Ahn, M. S., Ullrich, P. A., Gleckler, P. J., Lee, J., Ordonez, A. C., & Pendergrass, A. G. (2023). Evaluating precipitation distributions at regional scales: a benchmarking framework and application to CMIP5 and 6 models. *Geoscientific Model Development*, *16*(13), 3927–3951. doi: 10.5194/gmd-16-3927-2023

Akperov, M., Rinke, A., Mokhov, I. I., Semenov, V. A., Parfenova, M. R., Matthes, H., … Zhang, W. (2019). Future projections of cyclone activity in the Arctic for the 21st century from regional climate models (Arctic-CORDEX). *Global and Planetary Change*, *182*(April). doi: 10.1016/j.gloplacha.2019.103005

Allan, R. P., Soden, B. J., John, V. O., Ingram, W., & Good, P. (2010). Current changes in tropical precipitation. *Environmental Research Letters*, *5*(2). doi: 10.1088/1748-9326/5/2/025205

Beucher, S., & Lantuejoul, C. (1979). Use of Watersheds in Contour Detection. In *International workshop on image processing: Real-time edge and motion detection/estimation* (pp. 12–21). Retrieved from `http://cmm.ensmp.fr/{~}beucher/publi/watershed.pdfhttp://www.citeulike.org/group/7252/article/4083187`

Blázquez, J., & Solman, S. A. (2018). Fronts and precipitation in CMIP5 models for the austral winter of the Southern Hemisphere. *Climate Dynamics*, *50*(7-8), 2705–2717. doi: 10.1007/s00382-017-3765-z

Catto, J. L., Jakob, C., Berry, G., & Nicholls, N. (2012, may). Relating global precipitation to atmospheric fronts. *Geophysical Research Letters*, *39*(10), 1–6. Retrieved from https://onlinelibrary.wiley.com/doi/full/10.1029/2012GL051736https://onlinelibrary.wiley.com/doi/abs/10.1029/2012GL051736https://agupubs.onlinelibrary.wiley.com/doi/10.1029/2012GL051736http://doi.wiley.com/10.1029/2012GL051736 doi: 10.1029/2012GL051736

Catto, J. L., Madonna, E., Joos, H., Rudeva, I., Simmonds, I., Science, C., … Simmonds, I. (2015). Global relationship between fronts and warm conveyor belts and the impact on extreme precipitation. *Journal of Climate*, *28*(21), 8411–8429. doi: 10.1175/JCLI-D-15-0171.1

Catto, J. L., Nicholls, N., Jakob, C., & Shelton, K. L. (2014, nov). Atmospheric fronts in current and future climates. *Geophysical Research Letters*, *41*(21), 7642–7650. Retrieved from https://agupubs.onlinelibrary.wiley.com/doi/10.1002/2014GL061943 doi: 10.1002/2014GL061943

Catto, J. L., & Pfahl, S. (2013, oct). The importance of fronts for extreme precipitation. *Journal of Geophysical Research Atmospheres*, *118*(19), 10,791–10,801. Retrieved from https://onlinelibrary.wiley.com/doi/full/10.1002/jgrd.50852https://onlinelibrary.wiley.com/doi/abs/10.1002/jgrd.50852https://agupubs.onlinelibrary.wiley.com/doi/10.1002/jgrd.50852http://doi.wiley.com/10.1002/jgrd.50852 doi: 10.1002/jgrd.50852

Chou, C., Chiang, J. C., Lan, C. W., Chung, C. H., Liao, Y. C., & Lee, C. J. (2013). Increase in the range between wet and dry season precipitation. *Nature Geoscience*, *6*(4), 263–267. doi: 10.1038/ngeo1744

Dacre, H. F., Clark, P. A., Martinez-Alvarado, O., Stringer, M. A., & Lavers, D. A. (2015, aug). How Do Atmospheric Rivers Form? *Bulletin of the American Meteorological Society*, *96*(8), 1243–1255. Retrieved from https://journals.ametsoc.org/view/journals/bams/96/8/bams-d-14-00031.1.xmlhttps://journals.ametsoc.org/doi/10.1175/BAMS-D-14-00031.1 doi: 10.1175/BAMS-D-14-00031.1

Dai, A. (2006, sep). Precipitation Characteristics in Eighteen Coupled Climate Models. *Journal of Climate*, *19*(18), 4605–4630. Retrieved from http://journals.ametsoc.org/doi/10.1175/JCLI3884.1 doi: 10.1175/JCLI3884.1

Dai, A., Rasmussen, R. M., Liu, C., Ikeda, K., & Prein, A. F. (2020, jul). A new mechanism for warm-season precipitation response to global warming based on convection-permitting simulations. *Climate Dynamics*, *55*(1-2), 343–368. Retrieved from http://link.springer.com/10.1007/s00382-017-3787-6 doi: 10.1007/s00382-017-3787-6

Danabasoglu, G., Lamarque, J. F., Bacmeister, J., Bailey, D. A., DuVivier, A. K., Edwards, J., … Strand, W. G. (2020). The Community Earth System Model Version 2 (CESM2). *Journal of Advances in Modeling Earth Systems*, *12*(2), 1–35. doi: 10.1029/2019MS001916

Douville, H., Raghavan, K., Renwick, J., Allan, R., Arias, P., Barlow, M., … Zolina, O. (2023, jul). Water Cycle Changes [Book Section]. In V. Masson-Delmotte et al. (Eds.), *Climate change 2021 – the physical science basis* (pp. 1055–1210). Cambridge, United Kingdom and New York, NY, USA: Cambridge University Press. Retrieved from https://www.cambridge.org/core/product/identifier/9781009157896{\%}23c8/type/book{_}part doi: 10.1017/9781009157896.010

Dowdy, A. J., & Catto, J. L. (2017, jan). Extreme weather caused by concurrent cyclone, front and thunderstorm occurrences. *Scientific Reports*, *7*(1), 1–8. Retrieved from http://dx.doi.org/10.1038/srep40359https://www.nature.com/articles/srep40359 doi: 10.1038/srep40359

Drijfhout, S., van Oldenborgh, G. J., & Cimatoribus, A. (2012). Is a decline of AMOC causing the warming hole above the North Atlantic in observed and modeled warming patterns? *Journal of Climate*, *25*(24), 8373–8379. doi: 10.1175/JCLI-D-12-00490.1

Feng, Z., Houze, R. A., Leung, L. R., Song, F., Hardin, J. C., Wang, J., ... Homeyer, C. R. (2019). Spatiotemporal characteristics and large-scale environments of mesoscale convective systems east of the rocky mountains. *Journal of Climate*, *32*(21), 7303–7328. doi: 10.1175/JCLI-D-19-0137.1

Gershunov, A., Shulgina, T., Clemesha, R. E., Guirguis, K., Pierce, D. W., Dettinger, M. D., ... Ralph, F. M. (2019). Precipitation regime change in Western North America: The role of Atmospheric Rivers. *Scientific Reports*, *9*(1), 1–11. doi: 10.1038/s41598-019-46169-w

Gervais, M., Shaman, J., & Kushnir, Y. (2019). Impacts of the North Atlantic warming hole in future climate projections: Mean atmospheric circulation and the North Atlantic jet. *Journal of Climate*, *32*(10), 2673–2689. doi: 10.1175/JCLI-D-18-0647.1

Gervais, M., Shaman, J., & Kushnir, Y. (2020, may). Impact of the North Atlantic Warming Hole on Sensible Weather. *Journal of Climate*, *33*(10), 4255–4271. Retrieved from `https://journals.ametsoc.org/doi/10.1175/JCLI-D-19-0636.1` doi: 10.1175/JCLI-D-19-0636.1

Gettelman, A., Hannay, C., Bacmeister, J. T., Neale, R. B., Pendergrass, A. G., Danabasoglu, G., ... Mills, M. J. (2019). High Climate Sensitivity in the Community Earth System Model Version 2 (CESM2). *Geophysical Research Letters*, *46*(14), 8329–8337. doi: 10.1029/2019GL083978

Giorgi, F., Raffaele, F., & Coppola, E. (2019). The response of precipitation characteristics to global warming from climate projections. *Earth System Dynamics*, *10*(1), 73–89. doi: 10.5194/esd-10-73-2019

Govekar, P. D., Jakob, C., & Catto, J. (2014, jun). The relationship between clouds and dynamics in Southern Hemisphere extratropical cyclones in the real world and a climate model. *Journal of Geophysical Research: Atmospheres*, *119*(11), 6609–6628. Retrieved from `https://agupubs.onlinelibrary.wiley.com/doi/10.1002/2013JD020699` doi: 10.1002/2013JD020699

Hawcroft, M., Walsh, E., Hodges, K., & Zappa, G. (2018, nov). Significantly increased extreme precipitation expected in Europe and North America from extratropical cyclones. *Environmental Research Letters*, *13*(12), 124006. Retrieved from `https://iopscience.iop.org/article/10.1088/1748-9326/aaed59` doi: 10.1088/1748-9326/aaed59

Hawcroft, M. K., Shaffrey, L. C., Hodges, K. I., & Dacre, H. F. (2012, dec). How much Northern Hemisphere precipitation is associated with extratropical cyclones? *Geophysical Research Letters*, *39*(24), 1–7. Retrieved from `https://onlinelibrary.wiley.com/doi/abs/10.1029/2012GL053866https://agupubs.onlinelibrary.wiley.com/doi/10.1029/2012GL053866` doi: 10.1029/2012GL053866

Held, I. M., Soden, B. J., Oceanic, N., & Science, A. (2006, nov). Robust Responses of the Hydrological Cycle to Global Warming. *Journal of Climate*, *19*(21), 5686–5699. Retrieved from `http://journals.ametsoc.org/doi/10.1175/JCLI3990.1` doi: 10.1175/JCLI3990.1

Hénin, R., Ramos, A. M., Schemm, S., Gouveia, C. M., & Liberato, M. L. R. (2019, jan). Assigning precipitation to mid-latitudes fronts on sub-daily scales in the North Atlantic and European sector: Climatology and trends. *International Journal of Climatology*, *39*(1), 317–330. Retrieved from `https://onlinelibrary.wiley.com/doi/10.1002/joc.5808` doi: 10.1002/joc.5808

Hersbach, H., Bell, B., Berrisford, P., Hirahara, S., Horányi, A., Muñoz-Sabater, J., ... Thépaut, J. N. (2020). The ERA5 global reanalysis. *Quarterly Journal of the Royal Meteorological Society*, *146*(730), 1999–2049. doi: 10.1002/qj.3803

Klingaman, N. P., Martin, G. M., & Moise, A. (2017). ASoP (v1.0): A set of meth-

ods for analyzing scales of precipitation in general circulation models. *Geoscientific Model Development*, *10*(1), 57–83. doi: 10.5194/gmd-10-57-2017
Konstali, K., Spensberger, C., Spengler, T., & Sorteberg, A. (2024). Global attribution of precipitation to weather features. *Journal of Climate*, *37*(4), 1181 - 1196. Retrieved from https://journals.ametsoc.org/view/journals/clim/37/4/JCLI-D-23-0293.1.xml doi: 10.1175/JCLI-D-23-0293.1
Kooperman, G. J., Pritchard, M. S., & Somerville, R. C. J. (2014, sep). The response of US summer rainfall to quadrupled CO 2 climate change in conventional and superparameterized versions of the NCAR community atmosphere model. *Journal of Advances in Modeling Earth Systems*, *6*(3), 859–882. Retrieved from https://agupubs.onlinelibrary.wiley.com/doi/10.1002/2014MS000306 doi: 10.1002/2014MS000306
Laua, W. K., & Kim, K. M. (2015). Robust Hadley circulation changes and increasing global dryness due to CO2 warming from CMIP5 model projections. *Proceedings of the National Academy of Sciences of the United States of America*, *112*(12), 3630–3635. doi: 10.1073/pnas.1418682112
Lavers, D. A., Simmons, A., Vamborg, F., & Rodwell, M. J. (2022, oct). An evaluation of ERA5 precipitation for climate monitoring. *Quarterly Journal of the Royal Meteorological Society*, *148*(748), 3152–3165. Retrieved from https://onlinelibrary.wiley.com/doi/10.1002/qj.4351 doi: 10.1002/qj.4351
Mitchell, J. F., Wilson, C. A., & Cunnington, W. M. (1987). On Co2 climate sensitivity and model dependence of results. *Quarterly Journal of the Royal Meteorological Society*, *113*(475), 293–322. doi: 10.1002/qj.49711347517
Munday, C., & Washington, R. (2018). Systematic climate model rainfall biases over Southern Africa: Links to moisture circulation and topography. *Journal of Climate*, *31*(18), 7533–7548. doi: 10.1175/JCLI-D-18-0008.1
O'Brien, T. A., Risser, M. D., Loring, B., Elbashandy, A. A., Krishnan, H., Johnson, J., … Collins, W. D. (2020). Detection of atmospheric rivers with inline uncertainty quantification: TECA-BARD v1.0.1. *Geoscientific Model Development*, *13*(12), 6131–6148. doi: 10.5194/gmd-13-6131-2020
O'Brien, T. A., Wehner, M. F., Payne, A. E., Shields, C. A., Rutz, J. J., Leung, L. R., … Zhou, Y. (2022). Increases in Future AR Count and Size: Overview of the ARTMIP Tier 2 CMIP5/6 Experiment. *Journal of Geophysical Research: Atmospheres*, *127*(6), 1–15. doi: 10.1029/2021JD036013
O'Neill, B. C., Tebaldi, C., Van Vuuren, D. P., Eyring, V., Friedlingstein, P., Hurtt, G., … Sanderson, B. M. (2016). The Scenario Model Intercomparison Project (ScenarioMIP) for CMIP6. *Geoscientific Model Development*, *9*(9), 3461–3482. doi: 10.5194/gmd-9-3461-2016
Papritz, L., Pfahl, S., Sodemann, H., & Wernli, H. (2015). A climatology of cold air outbreaks and their impact on air-sea heat fluxes in the high-latitude South Pacific. *Journal of Climate*, *28*(1), 342–364. doi: 10.1175/JCLI-D-14-00482.1
Pendergrass, A. G., & Gerber, E. P. (2016). The rain is askew: Two idealized models relating vertical velocity and precipitation distributions in a warming world. *Journal of Climate*, *29*(18), 6445–6462. doi: 10.1175/JCLI-D-16-0097.1
Pfahl, S., O'Gorman, P. A., Fischer, E. M., O'Gorman, P. A., Fischer, E. M., O'Gorman, P. A., & Fischer, E. M. (2017, jun). Understanding the regional pattern of projected future changes in extreme precipitation. *Nature Climate Change*, *7*(6), 423–427. Retrieved from http://www.nature.com/articles/nclimate3287https://www.nature.com/articles/nclimate3287 doi: 10.1038/nclimate3287
Polade, S. D., Pierce, D. W., Cayan, D. R., Gershunov, A., & Dettinger, M. D. (2014). The key role of dry days in changing regional climate and precipitation regimes. *Scientific Reports*, *4*, 1–8. doi: 10.1038/srep04364
Prein, A. F., Mooney, P. A., Done, J., Prein, A. F., & Done, J. M. (2023). The Multi-Scale Interactions of Atmospheric Phenomenon in Extreme and

Mean Precipitation. , 1–22. Retrieved from https://doi.org/10.22541/essoar.167591088.85086118/v1 doi: 10.1029/2023EF003534

Priestley, M. D. K., & Catto, J. L. (2022). Future changes in the extratropical storm tracks and cyclone intensity, wind speed, and structure. *Weather and Climate Dynamics*, *3*(1), 337–360. doi: 10.5194/wcd-3-337-2022

Ritzhaupt, N., & Maraun, D. (2023). Consistency of Seasonal Mean and Extreme Precipitation Projections Over Europe Across a Range of Climate Model Ensembles. *Journal of Geophysical Research: Atmospheres*, *128*(1). doi: 10.1029/2022JD037845

Rodgers, K. B., Lee, S. S., Rosenbloom, N., Timmermann, A., Danabasoglu, G., Deser, C., … Yeager, S. G. (2021). Ubiquity of human-induced changes in climate variability. *Earth System Dynamics*, *12*(4), 1393–1411. doi: 10.5194/esd-12-1393-2021

Rüdisühli, S., Sprenger, M., Leutwyler, D., Schär, C., & Wernli, H. (2020). Attribution of precipitation to cyclones and fronts over Europe in a kilometer-scale regional climate simulation. *Weather and Climate Dynamics*, *1*(2), 675–699. doi: 10.5194/wcd-1-675-2020

Rutz, J. J., Shields, C. A., Lora, J. M., Payne, A. E., Guan, B., Ullrich, P., … Viale, M. (2019, dec). The Atmospheric River Tracking Method Intercomparison Project (ARTMIP): Quantifying Uncertainties in Atmospheric River Climatology. *Journal of Geophysical Research: Atmospheres*, *124*(24), 13777–13802. Retrieved from https://onlinelibrary.wiley.com/doi/10.1029/2019JD030936 doi: 10.1029/2019JD030936

Scheff, J., & Frierson, D. M. W. (2012, sep). Robust future precipitation declines in CMIP5 largely reflect the poleward expansion of model subtropical dry zones. *Geophysical Research Letters*, *39*(18), 1–6. Retrieved from https://agupubs.onlinelibrary.wiley.com/doi/10.1029/2012GL052910 doi: 10.1029/2012GL052910

Shields, C. A., Payne, A. E., Shearer, E. J., Wehner, M. F., O'Brien, T. A., Rutz, J. J., … Zarzycki, C. (2023). Future Atmospheric Rivers and Impacts on Precipitation: Overview of the ARTMIP Tier 2 High-Resolution Global Warming Experiment. *Geophysical Research Letters*, *50*(6), 1–9. doi: 10.1029/2022GL102091

Spensberger, C. (2024). *Dynlib: A library of diagnostics, feature detection algorithms, plotting and convenience functions for dynamic meteorology.* Zenodo. doi: 10.5281/zenodo.10471187

Spensberger, C., Konstali, K., & Spengler, T. (2024, March). *Moisture transport axes: a unifying definition for monsoon air streams, atmospheric rivers, and warm moist intrusions.* Retrieved from http://dx.doi.org/10.22541/essoar.170957480.06815908/v1 doi: 10.22541/essoar.170957480.06815908/v1

Spensberger, C., & Sprenger, M. (2018). Beyond cold and warm: an objective classification for maritime midlatitude fronts. *Quarterly Journal of the Royal Meteorological Society*, *144*(710), 261–277. doi: 10.1002/qj.3199

Sprenger, M., Fragkoulidis, G., Binder, H., Croci-Maspoli, M., Graf, P., Grams, C. M., … Wernli, H. (2017, aug). Global Climatologies of Eulerian and Lagrangian Flow Features based on ERA-Interim. *Bulletin of the American Meteorological Society*, *98*(8), 1739–1748. Retrieved from https://journals.ametsoc.org/doi/10.1175/BAMS-D-15-00299.1 doi: 10.1175/BAMS-D-15-00299.1

Stephens, G. L., L'Ecuyer, T., Forbes, R., Gettlemen, A., Golaz, J. C., Bodas-Salcedo, A., … Haynes, J. (2010). Dreary state of precipitation in global models. *Journal of Geophysical Research Atmospheres*, *115*(24), 1–14. doi: 10.1029/2010JD014532

Stevens, B., & Bony, S. (2013, may). What Are Climate Models Missing? *Science*, *340*(6136), 1053–1054. Retrieved from https://direct.mit.edu/

books/book/4262/chapter/179254https://www.science.org/doi/10.1126/science.1237554 doi: 10.1126/science.1237554

Sun, Y., Solomon, S., Dai, A., & Portmann, R. W. (2007, oct). How Often Will It Rain? *Journal of Climate*, *20*(19), 4801–4818. Retrieved from https://journals.ametsoc.org/view/journals/clim/20/19/jcli4263.1.xml doi: 10.1175/JCLI4263.1

Thackeray, C. W., DeAngelis, A. M., Hall, A., Swain, D. L., & Qu, X. (2018). On the Connection Between Global Hydrologic Sensitivity and Regional Wet Extremes. *Geophysical Research Letters*, *45*(20), 11,343–11,351. doi: 10.1029/2018GL079698

Thomas, C. M., & Schultz, D. M. (2019). What are the best thermodynamic quantity and function to define a front in gridded model output? *Bulletin of the American Meteorological Society*, *100*(5), 873–896. doi: 10.1175/BAMS-D-18-0137.1

Trenberth, K. E., Dai, A., Rasmussen, R. M., & Parsons, D. B. (2003, sep). The Changing Character of Precipitation. *Bulletin of the American Meteorological Society*, *84*(9), 1205–1217+1161. Retrieved from http://journals.ametsoc.org/doi/10.1175/BAMS-84-9-1205https://journals.ametsoc.org/doi/10.1175/BAMS-84-9-1205 doi: 10.1175/BAMS-84-9-1205

Utsumi, N., Kim, H., Kanae, S., & Oki, T. (2016, sep). Which weather systems are projected to cause future changes in mean and extreme precipitation in CMIP5 simulations? *Journal of Geophysical Research: Atmospheres*, *121*(18), 238–238. Retrieved from https://www.nature.com/articles/175238c0https://agupubs.onlinelibrary.wiley.com/doi/10.1002/2016JD024939 doi: 10.1002/2016JD024939

Utsumi, N., Kim, H., Kanae, S., & Oki, T. (2017, jan). Relative contributions of weather systems to mean and extreme global precipitation. *Journal of Geophysical Research: Atmospheres*, *122*(1), 152–167. Retrieved from http://doi.wiley.com/10.1002/2016JD025222https://agupubs.onlinelibrary.wiley.com/doi/10.1002/2016JD025222 doi: 10.1002/2016JD025222

Wernli, H., & Schwierz, C. (2006). Surface cyclones in the ERA-40 dataset (1958-2001). Part I: Novel identification method and global climatology. *Journal of the atmospheric sciences*, 2486–2507. Retrieved from http://journals.ametsoc.org/doi/abs/10.1175/JAS3766.1

Zappa, G., Hawcroft, M. K., Shaffrey, L., Black, E., & Brayshaw, D. J. (2015). Extratropical cyclones and the projected decline of winter Mediterranean precipitation in the CMIP5 models. *Climate Dynamics*, *45*(7-8), 1727–1738. Retrieved from http://dx.doi.org/10.1007/s00382-014-2426-8 doi: 10.1007/s00382-014-2426-8

Zappa, G., Shaffrey, L. C., Hodges, K. I., Sansom, P. G., & Stephenson, D. B. (2013, aug). A multimodel assessment of future projections of north atlantic and european extratropical cyclones in the CMIP5 climate models. *Journal of Climate*, *26*(16), 5846–5862. Retrieved from http://journals.ametsoc.org/doi/10.1175/JCLI-D-12-00573.1 doi: 10.1175/JCLI-D-12-00573.1